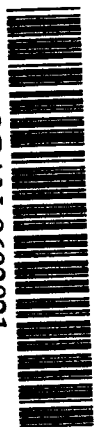


BB

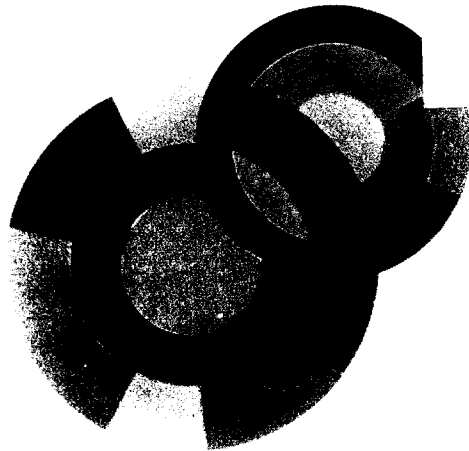
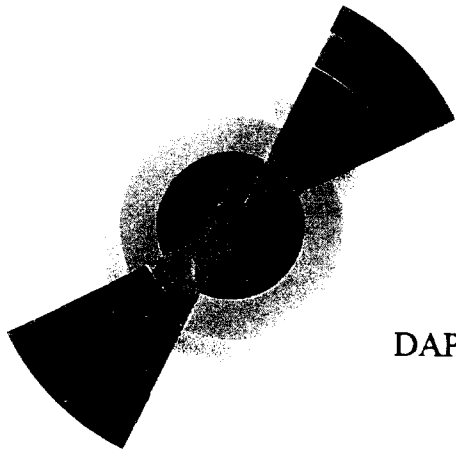


509640

SCAN-9603021



CERN LIBRARIES, GENEVA



DAPNIA/SPhN 95-45

07/1995

Dissipative aspects in 200 MeV/u Kr-induced reactions

DAPNIA

C. Donzaud, L. Tassan-Got, C. Stephan, D. Bachelier,
C.O. Bacri, R. Bimbot, B. Borderie, J.L. Boyard, F. Clapier,
T. Hennino, M.F. Rivet, P. Roussel, D. Bazin, C. Grunberg,
D. Disler, B. Lott, C. Volant

Le DAPNIA (Département d'Astrophysique, de physique des Particules, de physique Nucléaire et de l'Instrumentation Associée) regroupe les activités du Service d'Astrophysique (SAp), du Département de Physique des Particules Élémentaires (DPhPE) et du Département de Physique Nucléaire (DPhN).

Adresse : DAPNIA, Bâtiment 141
CEA Saclay
F - 91191 Gif-sur-Yvette Cedex

Soumis à Nuclear Physics A.

Dissipative aspects in 200 MeV/u Kr-induced reactions

C. Donzaud¹, L. Tassan-Got¹, C. Stéphan¹, D. Bachelier¹†, C.O. Bacri¹, R. Bimbot¹, B. Borderie¹, J.L. Boyard¹, F. Clapier¹, T. Hennino¹, M.F. Rivet¹, P. Roussel¹, D. Bazin^{2*}, C. Grunberg³, D. Disdier⁴, B. Lott^{4**}, C. Volant⁵

(1) Institut de Physique Nucléaire, B.P. 1, F-91406 Orsay, France

(2) Université Bordeaux 1, Domaine du Haut Vigneau, CENBG, F-33175 Gradignan Cedex, France

(3) GANIL, B.P. 5027, F-14021 Caen, France

(4) Centre de Recherches Nucléaires, F-67037 Strasbourg, France

(5) CEA DAPNIA/SPhN CE Saclay, 91191 Gif sur Yvette Cedex, France

ABSTRACT

Energy dissipation is studied in 200 MeV/u ⁸⁴Kr-induced reactions. Two experiments were performed at the SATURNE facility with the SPES4 spectrometer. Projectile-like fragments were measured for both the ⁸⁴Kr+¹⁹⁷Au and ⁸⁴Kr+⁵⁹Co systems. In the latter case light charged particles emitted in forward direction were detected in coincidence with PLF. From the projectile-like fragment isotopic distributions one can estimate that the mean excitation energy value per abraded nucleon deposited in primary fragments is quite large (20-30 MeV). However the excitation energy distribution is very broad : the neutron-rich nuclei come from weakly excited neutron-rich primary fragments. The mean velocity loss of projectile-like fragments with respect to the projectile velocity as well as the correlation between the proton coincidence rate and the projectile-like fragments momentum also claim for a dissipative mechanism.

KEYWORDS

Nuclear reaction ¹⁹⁷Au, ⁵⁹Co(⁸⁴Kr,X), E=200 MeV/nucleon, projectile-like fragment isotopic distribution, projectile-like fragment momentum, proton coincidence rates, excitation energy distribution, neutron-rich nucleus production, intranuclear-cascade model, statistical abrasion model, Goldhaber's model.

† *deceased*

* *present address MSU NSCL, East Lansing, Michigan 48824 USA*

** *present address GANIL B.P. 5027, F-14021 Caen, France*

1. Introduction

Peripheral collisions involving heavy ions at relativistic energies were first studied twenty years ago [1]. These first generation experiments already showed that the projectile residues populate the nuclear chart far from the β -stability valley [2], [3]. In the last five years the availability of ion beams with larger atomic numbers at SATURNE [4] and GSI [5], [6] facilities gave rise to a new spring of reaction mechanism studies.

Most of these studies are strongly tied to the assumption of a two-step reaction [7]. In a first stage, nucleon-nucleon fast collisions lead to excited projectile-like and target-like fragments which are accompanied by light particle emission. These two “hot” fragments are assumed to be thermalized before the de-excitation process which is the second slow stage of the collision. In peripheral reactions at relativistic energies, the excitation energy of primary fragments has a large average value but it is subject to large fluctuations so that its distribution widens to low values as well [6]. The study of the energy dissipation (i.e. of the amount of energy which is transferred from the incident relative motion to the internal energy of the fragments), its coupling to other quantities such as neutron-to-proton ratio and fragment linear velocity, give information on the underlying mechanism governing to a large extent the production yields. The aim of this paper is to get new insights into the dissipative processes in 200 MeV/u ^{84}Kr -induced reactions.

The excitation energy of the projectile-like fragments can be assessed from the effect of the evaporation stage on the N/Z ratio of these fragments [4], [8], [9] provided the projectile is heavy enough. Further inclusive experiments turn now to the study of specific channels ; fragments produced by removing one or two nucleons from the projectile are for instance of special interest since they are not affected by the evaporation stage and can probe the low excitation energy tail [6], [10].

We report here on two different experiments performed at the Saturne facility. In both experiments the projectile-like fragments, PLF, were detected with the SPES4 magnetic spectrometer. In the first inclusive one a Gold target was irradiated. In the second one a Cobalt target was used and Cesium-Iodide crystals were added in the reaction chamber to detect light charged particles in coincidence with PLF.

Before describing the experimental set-up, we will make some comments on the theoretical approach used to analyse the data. We will then show that the comparison of the measured PLF isotopic distributions with different models give reliable information on the excitation energy deposited in primary fragments. Exclusive data may shed more light on the fragmentation mechanism since they carry information not only on the mean energy deposited, but also on the excitation energy distribution. We will test this statement by looking at the correlation between proton coincidence rate and neutron-to-proton ratio of neutron-rich isotopes. In order to better characterize the dissipation process we will finally try to get new insights into the PLF momentum dispersion by studying the correlations

between these momenta and the proton coincidence rates.

2. Theoretical framework

A two-step model has been considered to describe these fragmentation reactions. The intranuclear-cascade model ISABEL [11] predicts the primary fragment distributions and the cascade particle emission (i.e. particles ejected by nucleon-nucleon collisions). The evaporation code LOTO [12] simulates the de-excitation of these primary fragments and gives the final projectile-like and target-like fragment distributions as well as the evaporated light particles.

The analysis of the exclusive experiment ($^{84}\text{Kr}+^{59}\text{Co}$) is based on the hypothesis that the detection of light charged particles can be tightly linked to the excitation energy deposited in PLF. This condition is fulfilled if these particles are mainly evaporation products from these PLF, that is, if they are not mixed with cascade particles. This assertion is based on the intranuclear-cascade model but our trust in the result depends on the ability of this calculation to adequately reproduce the cascade particles in the forward direction where the detectors were set up. As an example of the ability of this model to simulate the cascade particle emission, figure 1 shows the level of agreement which can be obtained from inclusive proton spectra at large angles where the emission of particles emitted from PLF evaporation is negligible. Experimental data are taken from Gosset et al. [13] and compared, without any renormalization factor, to the cascade particle components predicted by the calculation. The agreement supports the validity of this simulation to correctly describe the cascade particle emission.

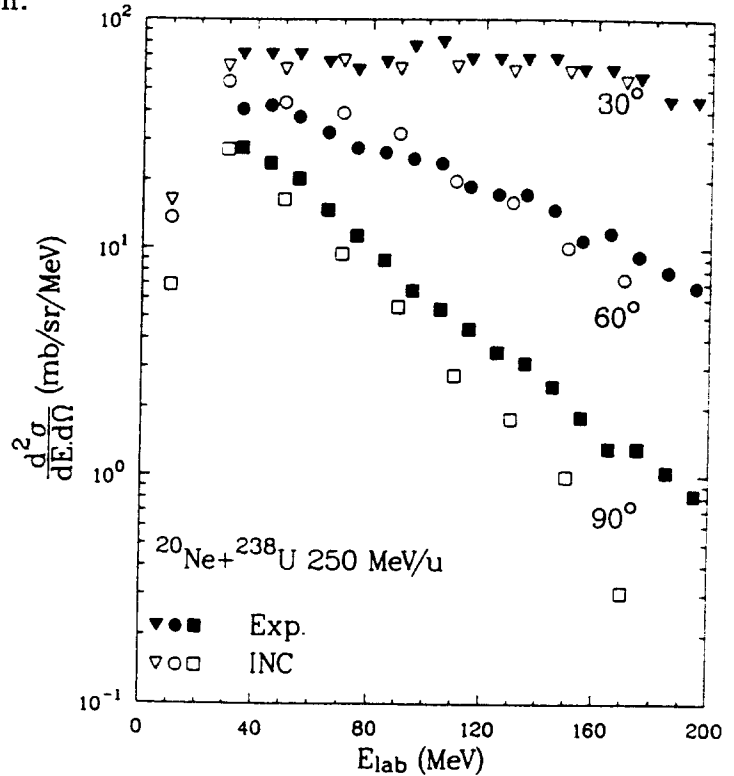


Figure 1 : Comparison of differential proton cross sections measured at different laboratory angles. Solid symbols : experimental data from [13]. Open symbols : cascade particle contribution from INC simulation.

In order to draw conclusions about the first stage of the collision from experimental data it is necessary to be as confident as possible in the calculation which simulates the de-excitation stage. The code LOTO we used is a Monte-Carlo simulation based on the following main ingredients :

- the transmission coefficients are the same as those from the LILITA code [14]
- the level density function is energy dependent : exponential at constant temperature at low energy [15] and a Fermi gas formula at high energy
- the level density parameter is taken from [16] ; it includes shell corrections but these corrections fade away exponentially when the excitation energy per nucleon increases. This last statement is described by a factor $e^{\frac{-E^*}{0.4\lambda}}$ where E^* is the excitation energy value inside the residual nucleus at each step of the decay chain.

A check of the validity of the LOTO calculation is shown in the following examples where we simulate the evaporation from ^{56}Ni and ^{58}Ni compound nuclei, at $E^* = 83$ MeV and 90 MeV respectively, resulting from ^{32}S induced fusion reactions [17]. Taken the measured fusion cross section σ_{fus} as an input in the calculation, the calculated mass and charge distributions of residual fragments reproduce within 20 %, and without any parameter adjustment, the measured individual yields (see figure 2). The validity of this evaporation code is then established around 1.5-2 MeV/u which is our domain of interest : the ISABEL calculation predicts a maximum in the excitation energy spectrum at about 2 MeV/u for primary fragments leading to a $Z=32$ final nucleus. The energy range extends from 1.6 to 3.3 MeV/u for a $Z=28$ fragment.

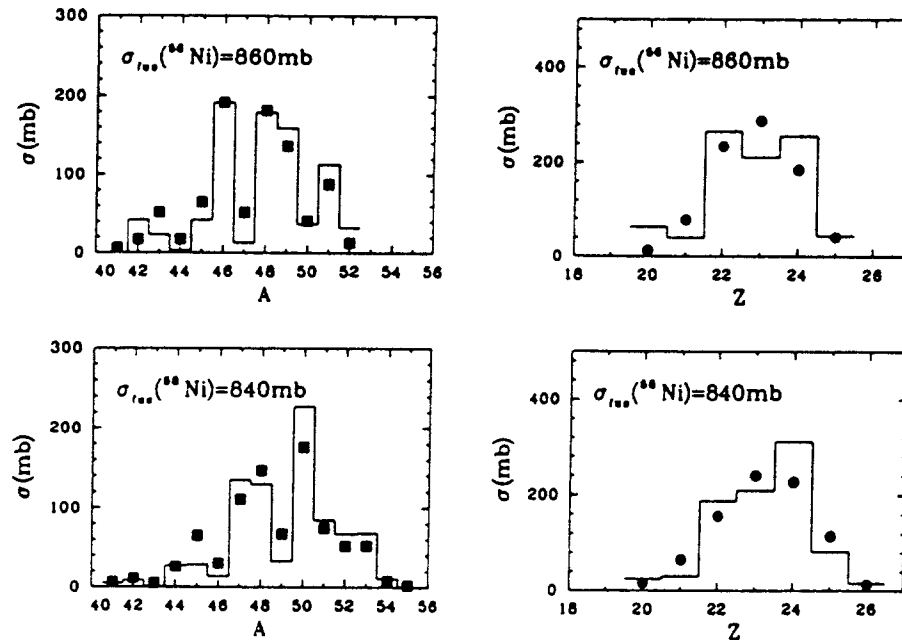


Figure 2 : Mass and charge distributions issued from the de-excitation of ^{56}Ni (upper part) and ^{58}Ni (lower part). Experimental data (symbols) are from [17] ; full lines result from LOTO simulation. Calculated errors are within the size of the symbols.

We compared [18] this evaporation code LOTO to the analytical calculation CASCADE [17], [19] and to the widely used code PACE [20], [21] for different Selenium isotopes at 200 MeV excitation energy and $5\hbar$ angular momentum. Whereas the LOTO and CASCADE simulations predict the same mean number of evaporated neutrons for all elements, the code PACE foresees one neutron less for most of the final elements.

3. Experimental set-up

The SPES4 magnetic spectrometer has a $0.6^\circ \times 1.2^\circ$ full aperture in plane and out of plane respectively. In the first inclusive experiment [4] with a 100 mg/cm^2 ^{197}Au target the spectrometer was successively set at two angles, 0.6° and 1.5° , i.e. inside and outside the grazing angle (0.97°). In the second experiment the ^{84}Kr beam was impinging on a 93 mg/cm^2 ^{59}Co target tilted at 45° with respect to the beam direction. The mean detection angle for fragments was then set at 0° to achieve the best efficiency.

During both experiments, the beam intensity was of some 10^5 particles per burst. Each burst lasted 300 ms during the 1.2 s cycle time. As the set-up for heavy fragments is already described elsewhere [4] we briefly summarize it here. Two position sensitive parallel plate avalanche counters (PPAC) were mounted at the final focal plane position ; another one equipped with a double time pick-off was mounted at the intermediate focal plane. The fragment velocity was determined by measuring the time of flight between these two dispersive focal planes which are 16 meters apart. The double time pick-off enabled us to carry out two independent time of flight measurements, which helped to improve the velocity and mass resolutions. To determine the exact flight path length, which is sensitive to the incident angle within the finite aperture of the spectrometer, ray-tracing was performed by using information from an additional position sensitive PPAC placed in front of the last quadrupole magnet located before the final focal plane. The magnetic rigidity was determined by the horizontal position at the final focal plane.

The atomic number of the fragments was obtained from the specific energy loss in an ionization chamber located behind the last focal plane. In the second experiment we measured that 3% of the Krypton ions were not fully stripped after passing through the target. A stripping foil placed at the intermediate focal plane allowed rejection off-line of most of these ions : ray-tracing was used to distinguish between fragments which had changed or kept their charge state at this point. We found that 3% of the krypton-like ions incompletely stripped after the target kept their ionic charge when passing through a $6 \mu\text{m}$ Titanium foil. Finally, by requiring that the charge state be constant along the whole path, one can estimate that 0.1% only of the detected fragments were hydrogen-like ones. This contamination which can give rise to ambiguities in the mass identification of isotopes, is lower for lighter fragments. The following resolutions (FWHM) were finally obtained : $A/\Delta A \simeq 140$ and $Z/\Delta Z \simeq 100$.

Two 14 cm thick Cesium-Iodide (CsI) crystals were dedicated to the detection of light

charged particles. They were placed symmetrically relative to the beam axis in the reaction chamber at 15 cm away from the target. Each of them was spanning a 5° to 10° range of polar angles from the beam direction and each of them subtended a 20 msr solid angle. A 1 cm thick plastic scintillator installed in front of each CsI crystal defined a restricted solid angle of 11 msr so that any straight trajectory coming from the target and crossing the side faces of the CsI crystals would be rejected. The particle identification was made by means of the rapid and slow components of the CsI signal coupled to the fast plastic signal.

Protons with energy larger than 238 MeV and most of deuterons punch through the CsI crystals. In the identification spectra these particles are mixed-up with particles which escape laterally from crystals. A simulation of multiple scattering based on a calculation from Eastham [22] and accounting for the slowing down of particles along their path inside the crystal, shows that 18 % of 200 MeV protons actually escape due to the Coulomb multiple scattering on crystal ions. On the other hand the pile-up rate in one crystal, deduced experimentally from the counting rates of events where the two identical CsI detectors are concerned, reached as much as 30 % for particles emitted in coincidence with a Cobalt fragment. Whereas the yield of the particles which laterally escape decreases when the detector surface acceptance increases, the pile-up rate demands a reduction of the exposed area : the geometry of the detectors used was finally a compromise between these two aspects.

The location of these detectors (between 5° and 10°) highly favored the detection of particles evaporated from PLF as indicated by simulations for protons in figure 3.

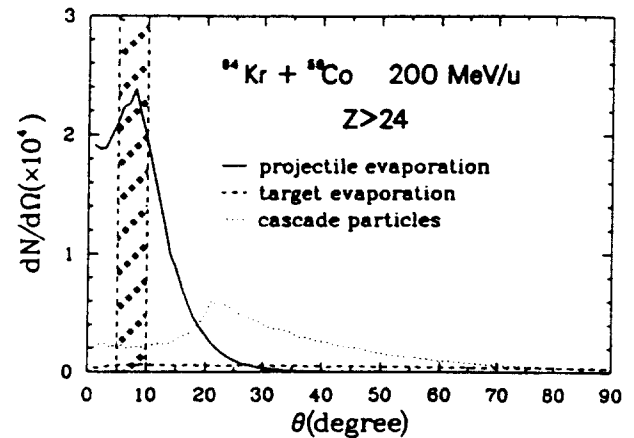
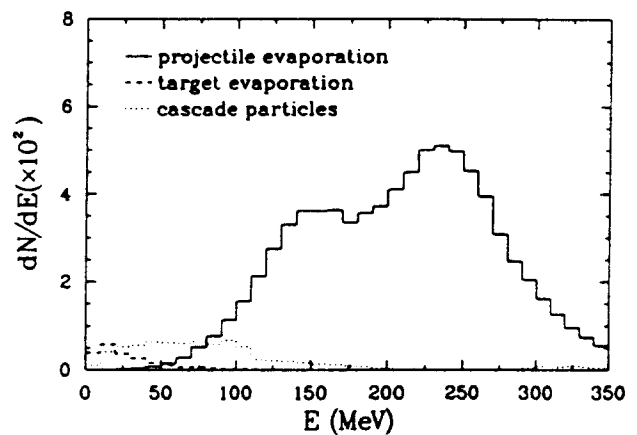


Figure 3: INC simulation coupled to LOTO calculation of proton contributions in coincidence with $Z > 24$ final fragments. Upper part : angular distributions for cascade and evaporation protons. The hatched area represents the angular range of the plastic scintillators. Lower part : energy spectra of protons expected to be detected in this angular domain.



These calculations were performed with the codes ISABEL and LOTO for the INC and evaporation stages respectively. They show, in angular distributions and energy spectra, the contributions of evaporation and cascade particle emission as detected in plastic detectors in coincidence with a heavy PLF.

According to these calculations, the measured protons in one telescope account for 2% of the total of the emitted protons in the collision. We verify that the calculated multiplicity (taken in the whole angular distribution of particles) presents for protons evaporated from PLF the same behavior than the calculated proton coincidence rate selected in the solid angle defined by plastic scintillators. These two arguments justify the assertion of a correlation between the detected proton coincidence rates and the excitation energy deposited in primary fragments.

4. Evaluation of the mean excitation energy

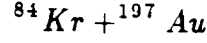
During the evaporation stage, fragments suffer an appreciable mass loss. After emitting some nucleons they populate the so-called evaporation "residue corridor" [23], an area of neutron-deficient nuclei where the proton and neutron emission probability values are almost equal. From inclusive experiments one can use the degree of equilibrium of the neutron-to-proton ratio towards this evaporation corridor to provide an excitation energy measurement as long as the projectile is heavy enough. This last restriction has been experimentally illustrated : an Ar-induced experiment has indeed shown that the isotopic distributions were not sensitive to the excitation energy owing to the N/Z ratio of the projectile close to unity [24].

Isotopic differential cross sections were extracted from inclusive data in the $^{84}\text{Kr} + ^{197}\text{Au}$ experiment [4] and compared to various calculations. A simulation based on the geometrical prescription of the participant-spectator model [25] shows that this model, where the lower limit of the excitation energy is calculated from the surface energy excess, underestimates the energy deposited in primary fragments by at least a factor of ten. For instance, the discrepancy amounts to three units in the most probable neutron number for the As isotopes [4]. Considering the excitation energy as a free parameter of the calculation, the amount of energy needed to reconcile experimental and calculated distributions reaches 20 MeV per abraded nucleon.

A more recent model from Gaimard and Schmidt called the statistical abrasion model [26] takes the same geometry as the participant-spectator model and uses the hypergeometrical prescription to calculate the primary isotopic distributions. Here the involved excitation energy comes from the mean energy induced by holes in the potential well below the Fermi surface, giving a mean excitation energy value of 13.3 MeV per abraded nucleon. In the intranuclear-cascade model ISABEL these holes are taken into account but the cascade particles which are captured in the nucleus potential well contribute to

the excitation energy calculation too. For comparison, in this last case the predicted value per abraded nucleon reaches 35 or 40 MeV on average for PLF produced from a ^{84}Kr beam at 200 MeV/u.

Figure 4 presents experimental mass distributions for some selected elements in the



experiment for the 0.6° (squares) and the 1.5° (circles) mean detection angles. The absolute differential cross sections which are shown are linked with the 0.6° mean detection angle; the measured distributions around 1.5° are normalized to those measured for the 0.6° mean detection angle with the factors shown in table 1. We can deduce from these ratio that all the elements with $Z \geq 27$ are preferentially produced in the selected angular domain inside the grazing angle. This tendency is enhanced for the elements near the projectile. Moreover all the displayed fragments in figure 4 are more neutron-deficient for the 1.5° mean detection angle. The discrepancy between the two explored angular domains is especially large for the nuclei $Z=34$ and $Z=35$.

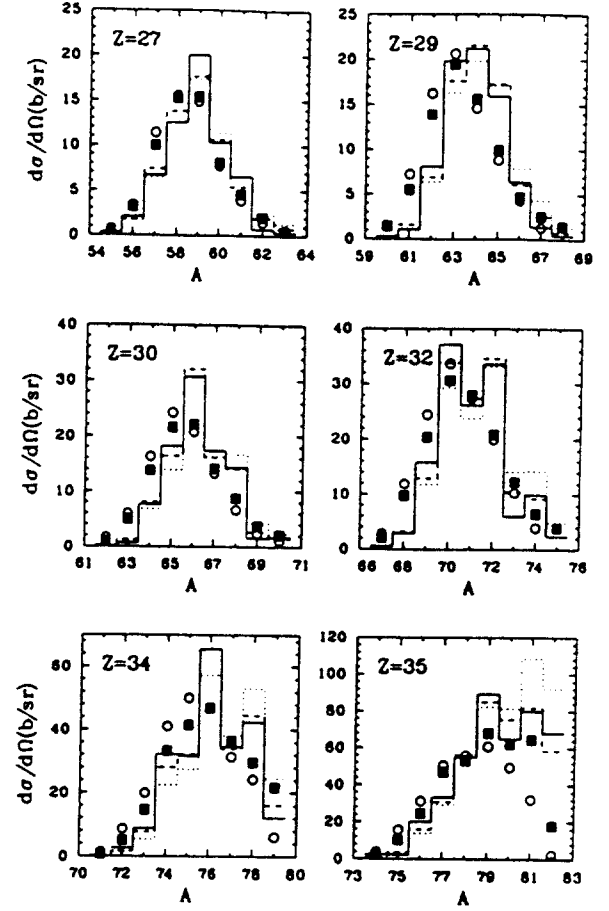


Figure 4 : Comparison between the experimental isotopic distributions from the $^{84}\text{Kr} + ^{197}\text{Au}$ system for the 0.6° mean detection angle (squares), the 1.5° mean detection angle (circles) and those predicted by ISABEL intranuclear-cascade model (full line), the statistical abrasion model (dotted line), this last model with twice the predicted excitation energy value (dashed line). Each primary calculation is coupled to the LOTO simulation. Measured yields for the angular domain around 1.5° are normalized to the experimental distribution for the 0.6° mean detection angle with the ratios displayed in table 1. Calculated yields are normalized to the same experimental distribution for each element. For the element $Z=35$ the normalization is made for isotopes with $A \leq 80$. For the most abundant isotope of each element relative statistical errors are about 2% for the statistical abrasion model and 7% for the INC model.

TABLE

Z	27	29	30	32	34	35
$\frac{d\sigma/d\Omega(1.5^\circ)}{d\sigma/d\Omega(0.6^\circ)}$	0.48	0.41	0.35	0.28	0.19	0.14

Table 1 : Ratio of the differential cross sections for the 0.6° and 1.5° mean detection angles for the elements displayed in figure 4

These features can be understood if one assumes that fragments detected around 1.5° correspond to primary collisions with a higher transverse momentum and consequently a higher excitation energy deposit. The subsequent evaporation stage favours then lower Z 's and depopulates the neutron-rich region.

The predictions of the INC calculation and the statistical abrasion model, both coupled to an evaporation step simulated by LOTO, are also shown in figure 4. In these simulations no angular selection was made in the PLF distributions. The statistical abrasion model leads to an overproduction of the neutron-rich isotopes. Since an increase of the excitation energy tends to depopulate the more neutron-rich isotopes and to enlarge the less neutron-rich fragment yields, one could think that a better agreement with data would be obtained with an excitation energy twice larger [8]. In fact, final nuclei are already populating the evaporation "residue corridor". Therefore a higher excitation energy could not increase the agreement with the data and, as a result, the microscopic INC model and the statistical abrasion one predict roughly the same isotopic distributions despite different excitation energy predictions. In the same way, if the excitation energy predicted by the INC calculation is artificially divided by a factor of 2 before applying the evaporation code, the agreement with the data does not change significantly.

Moreover we find [18] that the calculation describing the de-excitation process leads to different isotopic distributions according to the model : the tail of the neutron-deficient isotopes is underproduced by the simulation ISABEL coupled to LOTO and overproduced if the same calculation ISABEL is coupled to PACE. It is noticeable that the calculated yield of these nuclei is definitely influenced by the height of the Coulomb barrier governing the evaporation of protons and alpha particles.

The insensitivity of the isotopic distributions to the high excitation energy tail coupled to the uncertainties about evaporation codes limit the precision on the mean excitation energy value extracted from this method. An estimation of the mean excitation energy per abraded nucleon of 20-30 MeV seems however reasonable.

5. Incursion in the excitation energy spectrum

To gain a more quantitative insight into the excitation energy distribution, a measurement of proton coincidence rate was undertaken in the second experiment with the Cobalt target. This observable measured for each given isotope gives indications on the excitation energy of the primary fragment, hence it gives a hint on the pathway to its formation. We tried to explore the excitation energy distribution for specific isotopes, the neutron-rich ones. These nuclei can be produced in two ways :

i) The formation of cold primary fragments, followed by a short evaporation chain, could lead to final nuclei with a large N/Z ratio. These neutron-rich isotopes are then linked to a very low yield of protons evaporated from the projectile.

ii) On the other hand if primary fragments are rather excited, the only chance to get neutron-rich nuclei is to select a very specific evaporation path. In this case the yield of protons evaporated from the projectile is constant or even increases with the PLF mass for the most neutron-rich isotopes.

We have attempted to disentangle these two different mechanisms by looking at the proton coincidence rates. The measured coincidence rates for different isotopes are shown in figure 5 for six elements. The coincidence rate is defined as the ratio of the number of detected particles in plastic-CsI telescopes to the number of heavy fragments collected and identified in SPES4. Error bars include statistical errors only. Errors on the absolute coincidence rate values, including systematic errors, are larger (see below) but do not affect the accuracy of the relative coincidence rates between isotopes. These data show that the proton and alpha coincidence rates both increase when the observed element departs from the projectile. Moreover for a given element nuclei with large N/Z ratio are associated with low proton coincidence rates, especially for the highest Z 's. No dependence with the N/Z ratio of the fragment is seen for alpha coincidence rates. If most of the detected particles are evaporation products, as suggested by theoretical calculations, the measured decrease of the proton coincidence rates for the more neutron-rich nuclei is not consistent with the hypothesis ii) ; it rather exhibits that these nuclei come from weakly excited primary fragments.

Figure 6 displays the proton and alpha coincidence rates predicted by the INC simulation followed by the evaporation stage in the solid angle defined by the plastic scintillator. In this figure only particles evaporated from the projectile were displayed. Again, the simulation considers the whole angular distribution of projectile-like fragments whereas the measured fragments are taken between $\pm 0.3^\circ$ in plane and $\pm 0.6^\circ$ out of plane (for a grazing angle of 0.4°). It will be assumed subsequently that the detected PLF are representative of the whole production.

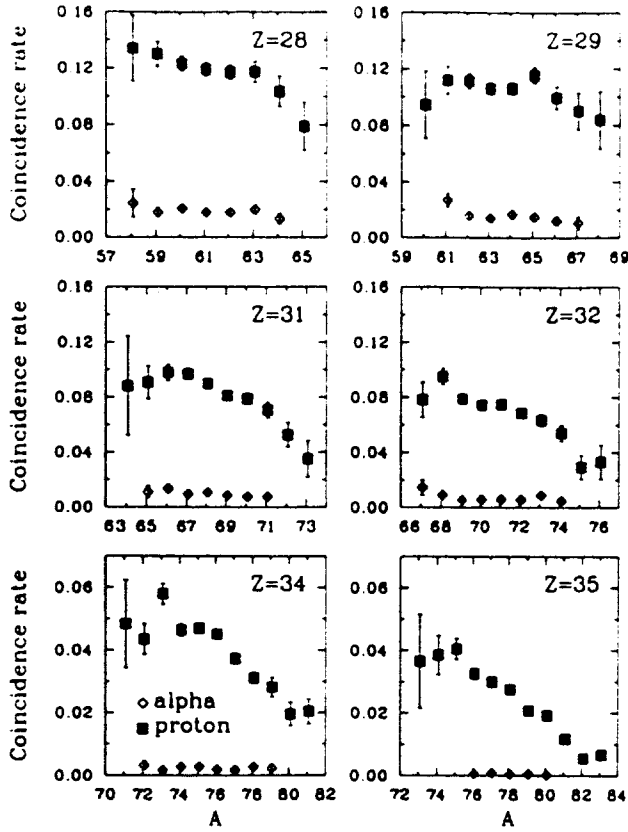


Figure 5 : *Experimental proton (squares) and alpha (dots) coincidence rates as function of mass for different elements in the $^{84}\text{Kr}+^{59}\text{Co}$ reaction.*

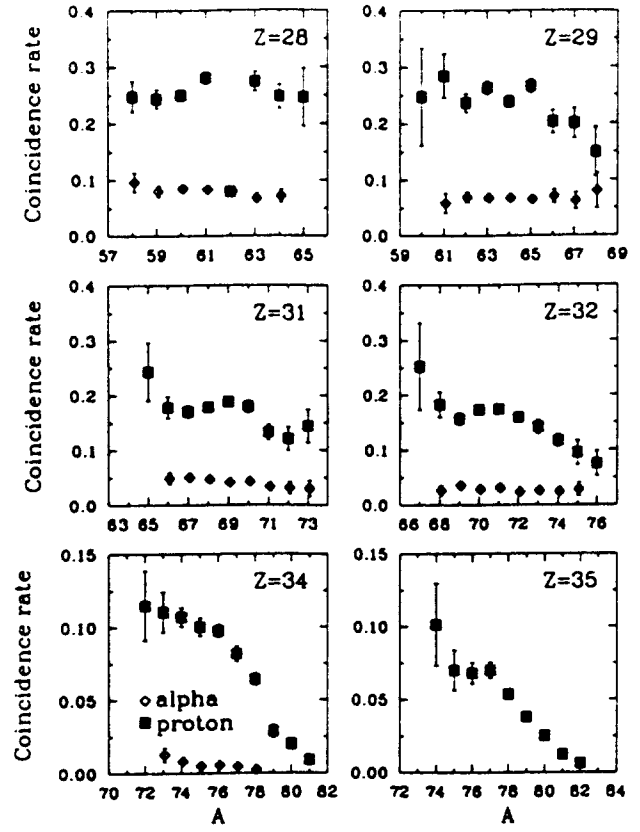


Figure 6 : *Proton (squares) and alpha (dots) coincidence rates as function of mass from INC simulation followed by LOTO calculation for the same elements as figure 5. Only PLF evaporation in the solid angle defined by the plastic scintillator is considered.*

The comparison of figures 5 and 6 exhibits a discrepancy between experimental and calculated absolute coincidence rates by a factor of 2. This factor can be ascribed to the rejection of pile-up particles in the same detector, and to the fact that experimental light particle detection angles are not known to an accuracy better than $\pm 1^\circ$. Evaporated particles being strongly forward focused, the detected coincidence rate and the α/p ratio steeply fall off when the detection angle increases ; the INC calculation foresees that a shift of the set-up by 2 degrees towards large angles is responsible for a 30% decrease of the coincidence rate. However an overestimation of the calculated excitation energy cannot be ruled out. In any case the excitation energy value which could be extracted from the proton coincidence rates seems roughly consistent with that obtained from the isotopic distributions.

The calculated proton coincidence rates follow the same trend as the data : overall increase of the coincidence rate when departing from the projectile, lowest coincidence rates associated with neutron-rich species. The comparison between the INC simulation and the data enlightens a specific feature of such calculations which has already been

pointed out [6] : the mean excitation energy deposited by cascade nucleons is large, but the spectrum is very broad, opening the possibility of cold primary fragment formation. The INC simulation foresees for instance a mean excitation energy value of 155 MeV for a ^{69}Ge isotope and only 57 MeV for the more neutron-rich ^{76}Ge isotope.

6. Correlation between the excitation energy and the PLF momentum

The large excitation energy deposited on average in primary fragments is then well established. Whereas the velocity loss of PLF with respect to the projectile velocity can clearly be assigned to a dissipative mechanism, the origin of the momentum dispersion P_{rms} is not yet well defined. The Goldhaber's prediction [27] foresees a P_{rms} value 20% higher on average than the experimental one for a given fragment mass [4], [28]. This discrepancy has recently been ascribed to the mass loss in the evaporation stage which is not taken into account in the model [29] ; this process increases indeed the velocity fluctuations but it decreases the fragment mass. On the other hand, Morrissey [30] stressed that the sequential decay of primary fragments cannot fully account for these widths and that the fast initial stage of the collision comes into play. Moreover the intranuclear-cascade model is able to correctly reproduce the PLF momentum width [4].

In the way of a better understanding of the underlying mechanism, it is relevant to test the Goldhaber's picture. Goldhaber showed that whatever the involved process (a sudden liberation of clusters with insignificant final state interaction or a break-up of a thermalized nucleus) the fragment momentum distribution is the same provided that the total momentum is conserved. The width of the longitudinal momentum distribution originates also only from fluctuations in momentum of nucleons which are removed throughout the process. He noticed himself that this statement is true as long as the momentum transfer between the projectile and the target is small enough.

A first way to test this model is to measure the velocity loss of the PLF as compared to the projectile velocity. For that purpose, the fragment velocity distributions were reconstructed event by event for the $^{84}\text{Kr}+^{197}\text{Au}$ experiment [18]. It appears that the mean velocity loss of fragments, though it is relatively weak (2% for an isotope with 40 nucleons less than the projectile), may lead to large dissipative energy values. This loss of velocity evokes a "friction" process where particles involved in the reaction transfer momentum by colliding with other particles. In the intranuclear-cascade model ISABEL such a friction is taken into account ; this model coupled to the LOTO simulation predicts also velocity loss values in good agreement with the experimental data [4].

In the Goldhaber's model the PLF velocity should be independent of the excitation energy deposited in fragments since the hypothesis of the momentum conservation is sufficient to reproduce the momentum dispersion. In order to test this picture more deeply we studied the correlation between the measured proton coincidence rates and the PLF

momenta. The velocity spectrum of each isotope has been divided into three parts as illustrated in figure 7. The central cut is limited to $\pm 0.7\sigma$, where σ is the standard deviation of the distribution, and the associated proton coincidence rate is plotted in figure 8 as solid stars. Trailing cuts are taken beyond $\pm\sigma$ and for corresponding coincidence rates open symbols are used.

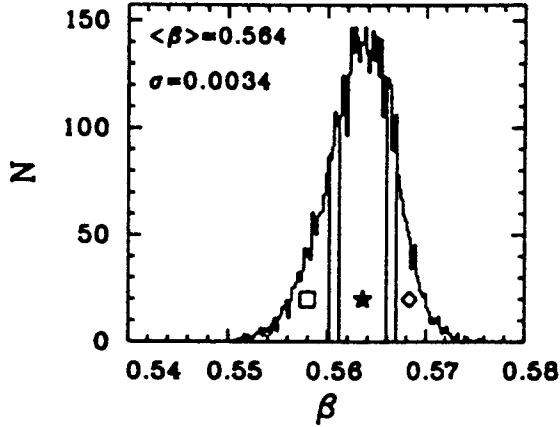


Figure 7 : Velocity distribution of the ^{74}As isotope for the $^{84}\text{Kr}+^{59}\text{Co}$ system. Three cuts in PLF momentum are defined, with the corresponding symbols used in figure 8 for the proton coincidence rates.

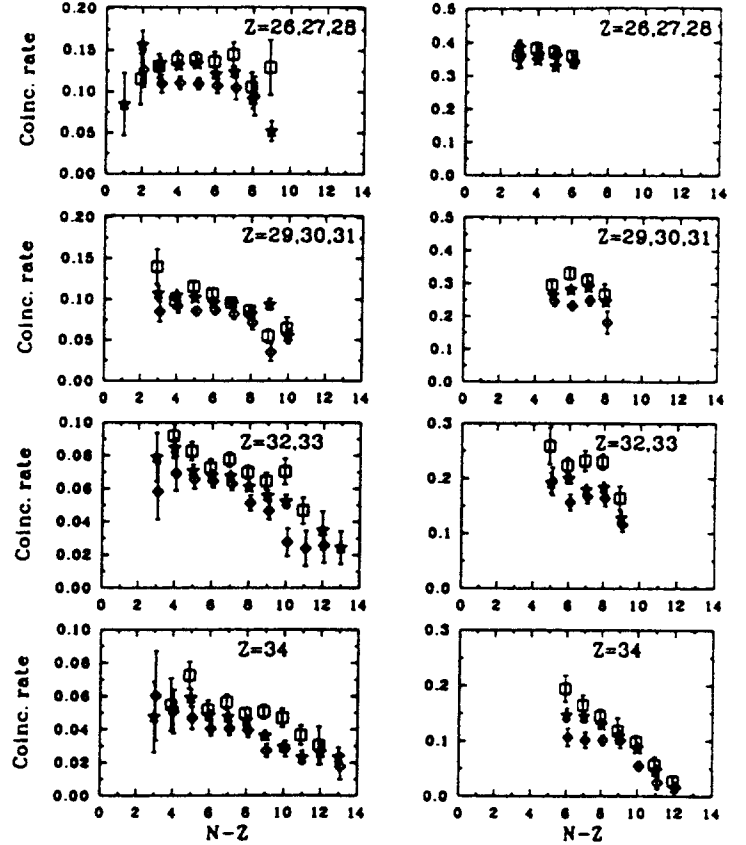


Figure 8 : Proton coincidence rates associated with three PLF velocity cuts shown in figure 7 for different fragments. Left column : experimental data. Right column : contribution of protons evaporated from the primary fragments, in the solid angle defined by the plastic detectors, predicted by INC simulation coupled to LOTO calculation. The coincidence rates related to the elements mentioned in each figure were added.

Figure 8 displays the experimental (left column) proton coincidence rates associated with these cuts versus the neutron excess number for four groups of elements. Experimental data reveal a dependence of the coincidence rate on the selected momentum band : lower momenta are associated with higher excitation energies. The intranuclear-cascade simulation whose results are depicted in the right column of figure 8, reproduces this trend.

This behavior shows that the kinematical recoil effects linked to the momentum conservation are not the only origin of the momentum dispersion and that friction effects take place by means of a momentum transfer between the target and the projectile, as we already pointed out from the PLF velocity loss.

7. Conclusion

Isotopic distributions of projectile-like fragments extracted from the $^{84}\text{Kr}+^{197}\text{Au}$ experiment show that peripheral collisions are largely dissipative at 200 MeV/u incident energy. This result agrees with experiments performed at higher incident energies and with heavier projectiles at the GSI facility [8], [31] ; it was also found there that inclusive data are well reproduced if an excitation energy between 20 and 30 MeV per abraded nucleon is considered.

These dissipative aspects can be studied with more details from the proton coincidence rates mirroring the excitation energy in fragments. These coincidence rates were sampled by using telescopes in coincidence with PLF in the $^{84}\text{Kr}+^{59}\text{Co}$ experiment. A clear correlation between the excitation energy and the projectile-like fragment momentum proves indeed that the momentum width cannot be fully explained without invoking a momentum transfer between projectile and target. Furthermore, we looked at neutron-rich nuclei to explore the excitation energy spectrum : these isotopes come from weakly excited primary fragments. Exotic nuclei production consequently demands large neutron-to-proton ratio and excitation energy fluctuations in the primary fragment distributions. It is finally interesting to stress that the intranuclear-cascade model seems to be a reliable framework to describe peripheral collisions at relativistic energies.

The authors would like to thank the accelerator crew of the Saturne facility for providing the Kr beams. They also thank the director of GANIL, S. Harar, for making the detector system attached to the SPEG spectrometer available for these experiments. The authors are indebted to D. J. Morrissey and K. Sümmerer for providing them with the intranuclear-cascade code ISABEL.

REFERENCES

- [1] *H. H. Heckman* Proc. 5th Intern. Conf. on High energy physics and nuclear structure, Uppsala, 1973, ed. G. Tibell (Almqvist and Wiksell, Uppsala, 1974) p403.
- [2] *T. J. M. Symons, Y. P. Viyogi, G. D. Westfall, P. Doll, D. E. Greiner, H. Faraggi, P. J. Lindstrom and D. K. Scott*, Phys. Rev. Lett. **42** (1979) 40.
- [3] *G. D. Westfall, T. J. M. Symons, D. E. Greiner, H. H. Heckman, P. J. Lindstrom, J. Mahomey, A. C. Shotter and D. K. Scott*, Phys. Rev. Lett. **43** (1979) 1859.
- [4] *C. Stéphan, L. Tassan-got, D. Bachelier, C. O. Bacri, R. Bimbot, B. Borderie, J. L. Boyard, F. Clapier, C. Donzaud, T. Hennino, M. F. Rivet, P. Roussel, D. Bazin, C. Grunberg, D. Disdier and B. Lott*, Phys. Lett. **B262** (1991) 6.
- [5] *M. Weber, C. Donzaud, J. P. Dufour, H. Geissel, A. Grewe, D. Guillemaud-Mueller, H. Keller, M. Lewitowicz, A. Magel, A. C. Mueller, G. Münzenberg, F. Nickel, M. Pfützner, A. Piechaczek, M. Pravikoff, E. Roeckl, K. Rykaczewski, M. G. Saint-Laurent, I. Schall, C. Stéphan, K. Sümmerer, L. Tassan-Got, D. J. Viera and B. Voss*, Z. Phys. **A343** (1992) 67.
- [6] *K. H. Schmidt, H. Geissel, G. Münzenberg, F. Nickel, M. Pfützner, C. Scheidenberger, K. Sümmerer, D. J. Viera, T. Brohm, H. G. Clerc, M. Dornik, M. Fauerbach, A. Grewe, E. Hanelt, A. Junghans, W. Morawek, B. Voss, C. Ziegler and A. Magel*, Nucl. Phys. **A542** (1992) 699.
- [7] *R. Serber*, Phys. Rev. **72** (1947) 1114.
- [8] *K. H. Schmidt, T. Brohm, H. G. Clerc, M. Dornik, M. Fauerbach, H. Geissel, A. Grewe, E. Hanelt, A. Junghans, W. Morawek, G. Münzenberg, F. Nickel, M. Pfützner, C. Scheidenberger, K. Sümmerer, D. J. Viera, B. Voss and C. Ziegler*, Phys. Lett. **B300** (1993) 313.
- [9] *T. Brohm, H. G. Clerc, M. Dornik, M. Fauerbach, J. J. Gaimard, A. Grewe, E. Hanelt, B. Voss, C. Ziegler, B. Blank, R. Del Moral, J. P. Dufour, L. Fauz, C. Marchand, M. S. Pravikoff, K. H. Schmidt, H. Geissel, G. Münzenberg, F. Nickel, M. Pfützner, E. Roeckl, I. Schall, K. Sümmerer, D. J. Viera and M. Weber*, Nucl. Phys. **A550** (1992) 540.
- [10] *M. Pfützner, S. Andriamonje, B. Blank, R. Del Moral, J. P. Dufour, A. Fleury, T. Josso, M. S. Pravikoff, T. Brohm, A. Grewe, E. Hanelt, A. Heinz, A. Junghans, C. Röhl, S. Steinhäuser, B. Voss, K. H. Schmidt, S. Czajkowski, Z. Janas, A. Piechaczek, E. Roeckl, K. Sümmerer, W. Trinder, M. Weber and M. Fauerbach*, Centre d'Etudes Nucléaires de Bordeaux-Gradignan report CENBG-9419 (1994), submitted to Nucl. Phys. A.
- [11] *Y. Yariv and Z. Fraenkel*, Phys. Rev. **C24** (1981) 488.
- [12] *L. Tassan-Got, C. Stéphan, C. O. Bacri, R. Bimbot, B. Borderie, J. L. Boyard, F. Clapier, T. Hennino, M. F. Rivet, P. Roussel, D. Disdier, C. Lott, D. Bazin, C. Grunberg*, Proc. XXVIII Winter Meeting on Nuclear Physics, Bormio, 1990, ed. Ric. Sci.

ed Educazione Permanente, suppl. 78 (1990) p. 361.

- [13] *J. Gosset, H. H. Gutbrot, W. G. Meyer, A. M. Poskanzer, A. Sandoval, R. Stock and G. W. Westfall*, Phys. Rev. C**16** (1977) 629.
- [14] *J. Gomez del Campo, R. G. Stokstadt, J. A. Biggerstaff, R. A. Dayras, A. H. Snell and P. H. Stelson*, Phys. Rev. C**19** (1979) 2170.
- [15] *D. N. Lang*, Nucl. Phys. **26** (1961) 434.
- [16] *A. Gilbert and A. G. W. Cameron*, Can. J. Phys. **43** (1965) 1446.
- [17] *F. Pühlhofer, W. F. W. Schneider, F. Busch, J. Barrette, P. Braun-Munzinger, C. K. Gelbke and H. E. Wegner*, Phys. Rev. C**16** (1977) 1010.
- [18] *C. Donzaud*, Ph.D. thesis, Université Paris XI, IPNO-T-93-05 (1993).
- [19] *T. Suomijarvi*, private communication (1993).
- [20] *A. Gavron*, Phys. Rev. C**21** (1980) 230.
- [21] *M. Morjean*, private communication (1993).
- [22] *D. A. Eastham*, Nucl. Inst. and Meth. **125** (1975) 277.
- [23] *J. P. Dufour, H. Delagrangé, R. Del Moral, A. Fleury, F. Hubert, Y. Llabador, M. B. Mauhourat, K. H. Schmidt and A. Lleres*, Nucl. Phys. A**387** (1982) 157c.
- [24] *D. J. Morrissey, L. F. Oliveira, J. O. Rasmussen and G. T. Seaborg*, Phys. Rev. Lett. **43** (1979) 1139.
- [25] *J. D. Bowman, W. J. Swiatecki and C. E. Tsang*, Lawrence Berkeley Laboratory report LBL-2908 (1973).
- [26] *J. J. Gaimard and K. H. Schmidt*, Nucl. Phys. A**531** (1991) 709.
- [27] *A. S. Goldhaber*, Phys. Lett. B**53** (1974) 306.
- [28] *D. E. Greiner, P. J. Lindstrom, H. H. Heckman, B. Cork and F. S. Bieser*, Phys. Rev. Lett. **35** (1975) 152.
- [29] *E. Hanelt, A. Grewe, K. H. Schmidt, T. Brohm, H. G. Clerc, M. Dornik, M. Fauerbach, H. Geissel, A. Magel, G. Münzenberg, F. Nickel, M. Pfützner, C. Scheidenberger, M. Steiner, K. Sümmerer, B. Voss, M. Weber, J. Weckenmann and C. Ziegler*, Z. Phys. A**346** (1993) 43.
- [30] *D. J. Morrissey*, Phys. Rev. C**39** (1989) 460.
- [31] *M. Weber, C. Donzaud, J. P. Dufour, H. Geissel, A. Grewe, D. Guillemaud-Mueller, H. Keller, M. Lewitowicz, A. Magel, A. C. Mueller, G. Münzenberg, F. Nickel, M. Pfützner, A. Piechaczek, M. Pravikoff, E. Roeckl, K. Rykaczewski, M. G. Saint-Laurent, I. Schall, C. Stéphan, K. Sümmerer, L. Tassan-Got, D. J. Viera and B. Voss*, Nucl. Phys. A**578** (1994) 659.